Effect of Soot Layer Microstructure on Diesel Particulate Filter Regeneration

Margaritis Kostoglou and Athanasios G. Konstandopoulos
Aerosol and Particle Technology Laboratory, CERTH/CPERI, P.O. Box 361, Thermi, Thessaloniki 57001, Greece

DOI 10.1002/aic.10484
Published online June 30, 2005 in Wiley InterScience (www.interscience.wiley.com).

Diesel particulate filter (DPF) behavior depends strongly on the microstructural properties of the deposited soot aggregates. In the past the issue of the growth process of soot deposits in honeycomb ceramic filters has been addressed under nonreactive conditions, and the influence of the filter operating conditions has been defined in terms of the dimensionless Peclet number. Appropriate soot cake microstructural descriptors are studied under reactive conditions for different oxidation modes. To this end the effect of deposit microstructure on the soot oxidation kinetics is investigated. Different microstructural models for the reacting soot deposit are examined in a unified fashion and a generalized constitutive equation is obtained, describing several modes of microstructure evolution (shrinking layer, shrinking density, discrete columnar and continuous columnar). Understanding the structural evolution of soot deposits during oxidation is of major importance for intelligent operation and simulation of DPFs, and for practical estimation of their soot mass load. © 2005 American Institute of Chemical Engineers *AIChE J,* 51: 2534–2546, 2005

Introduction

The use of DPF systems appears necessary for complying with heavy-duty engine emission standards within the next few years, while drive for higher market share and notions of environmental friendliness have already been shaping the modern diesel passenger car scene. The first commercially available vehicles equipped with DPFs were already introduced in 2001, and many offerings of DPF equipped car models debuted at the 2003 60th International Motor Show.[1]

These developments increase further the demand for advanced DPF simulation tools as is evidenced by the evolution of articles on DPF simulation published since the introduction of DPF technology in 1981 (Figure 1). Similar to the growth of a species filling an ecological niche the population of DPF simulation papers can be "modeled" by the logistic growth equation (sigmoid). Two phases can be seen; the early (1981 – 1995) and the recent (1996 –present), which is predicted to last until 2015. We are, thus, experiencing the most intense period of growth of the field!

The mutliscale nature of DPFs is well appreciated (Figure 2), and DPF simulation has been conveniently classified using the different spatial levels.[2] The basic simulation module employed most frequently is the single channel model developed by Bissett[3] and extended by Konstandopoulos and Kostoglou,[4,5] among others. In this approach a constant density, constant specific surface area soot deposit has been employed.

To improve on this approach, there are two directions for further study. The first direction through the so-called multichannel models[6,7] aims at an entire filter model and its integration with other models of components in the exhaust aftertreatment system (for example, diesel oxidation catalysts, NO_x traps, and so on). The second direction aims at a better understanding of the phenomena occurring at the level of soot nanoparticles, and their effects on the scale of the soot deposit thickness (deposit microstructure).

Deposit microstructure during the (nonreactive) DPF loading phase has been studied extensively by Konstandopoulos et al.[8] and it has been related to the fundamental mechanisms of particulate transport toward surfaces, and the competition between convection and diffusion.[9,10] The interaction between

Correspondence concerning this article should be addressed to A. G. Konstandopoulos at agk@cperi.certh.gr.

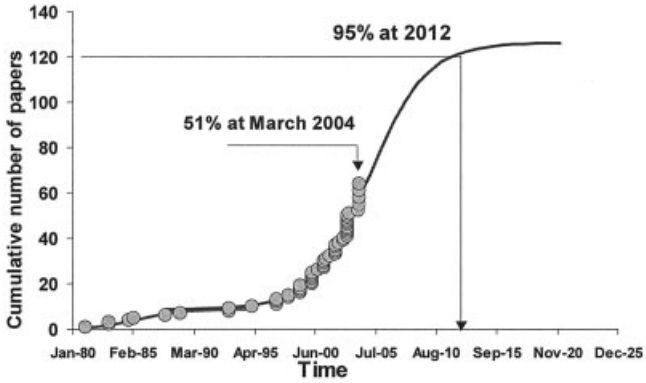

Figure 1. Evolution of publications on DPF simulation.

deposit microstructure and soot oxidation during the regeneration phase is a much more complicated issue and only few works in the literature have touched it.

The routine assumption is that the density and specific area of the deposit remain constant during its oxidative shrinkage. In general, the evolving radius of the primary particles in the soot aggregates, comprising the deposit, should lead in evolving deposit properties. The constant specific area assumption has been relaxed in the earlier note of Shadman,[11] which assumes that the deposits consist of linear columnar chains of spherical particles (one stacked on top of the other). The model is of discrete nature requiring equations to be written for each particle in the column. Considering the size of primary soot particles (typically between 20 and 40 nm), and a usual thickness for the deposit layer (tens of microns), this treatment would require the solution of a few thousand differential and algebraic equations. It is this small ratio between primary particle size and deposit thickness that enables the derivation of continuum soot deposit microstructural models.

Continuous models for the evolution of the soot deposit have been originally introduced by Bissett and Shadman[12] and Bissett.[13] The latter work provided an asymptotic analysis for the temperature distribution across the soot deposit, and showed that the governing dimensionless parameter (the thermal Peclet number) is sufficiently small to make the assumption of a uniform temperature across the soot deposit a very good approximation. In these works, the assumption of constant deposit properties was invoked. Furthermore, a convection term arising from the volumetric deposit shrinkage was not taken into account in the energy equation and the energy equation cited in these works refers to the case where the reactions take place exclusively at the deposit surface. Nevertheless, this omission of the convective term does not influence the asymptotic analysis performed by Bissett.[13] The recent study of Haralampous and Koltsakis[14] on the temperature distribution across the deposit also employs an energy equation that does not include the convective term due to the volumetric deposit shrinkage. For practical applications of diesel particulate filters a maximum soot load, an acceptable pressure drop and a total filter volume is imposed by design considerations. These considerations lead to thermal Peclet numbers (considering in a self-consistent manner variations of soot microstructure with flow) less than 0.03 and, therefore, the uniform temperature across the soot deposit layer remains a valid assumption.

Including discrete microstructural features in macroscopic regeneration models is not a trivial task, and it can lead to significant errors if it is not done consistently. The scope of this work is to clarify this issue through the development of self-consistent continuum microstructural models for the soot deposit oxidation process.

The structure of this work is as follows: First, the continuum one-dimensional (1-D) model, which describes the evolution of the local deposit properties during the regeneration process is formulated in terms of constitutive laws (rates) for the variation of deposit properties. Knowledge of the particle scale deposit evolution dynamics is necessary for the derivation of these constitutive laws. Four simple models of deposited particle evolution dynamics are studied and the corresponding constitutive laws are derived. It was found that all of them are subcases of a generalized microstructural model containing two parameters (microstructural descriptors). Then, analytical and/or approximate solutions are given for certain values of these two parameters, and a numerical method is developed for the treatment of the general case. Subsequently, several results are shown and discussed in order to assess the influence of the soot layer microstructure on the regeneration process for the cases of slow and fast regeneration separately. Finally, a comparison of the simulated soot deposit conversions with well-controlled experimental results with soot deposits grown on cake filter disks is performed.

Problem Formulation

General formulation

According to the continuum description developed here the soot deposit layer can be characterized by its thickness w, its density distribution $\rho(x)$ (g/cm^3), and its specific surface area distribution S(x) (cm^2/g). The variable x is the length across the deposit and is measured from the filter wall (x = 0) to the deposit surface (x = w). The continuum description implies that the soot layer is uniform along the directions parallel to the porous wall surface at least over the size scale of its thickness.

Since the scope here is to examine the influence of the deposit structure on the regeneration process, the following simple first-order heterogeneous soot oxidation reaction is considered for simplicity. Finite CO selectivity[2,4] does not qualitatively change the picture

$$C + O_2 \rightarrow CO_2$$

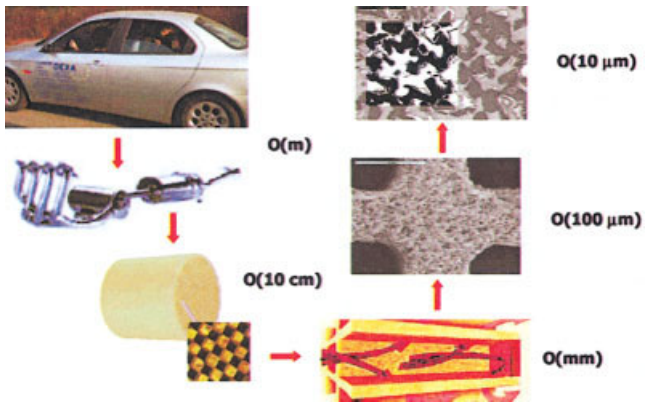

Figure 2. Multiscale nature of DPF simulation.

The timescales of the soot oxidation and of the inlet flow transients are much larger than the residence time of the gas in the soot layer, so the following local quasi-steady oxygen balance across the soot layer can be written

$$v\frac{dY}{dx} = KS\rho Y \tag{1}$$

where Y is the local mass fraction of oxygen in the exhaust gas, v is the filtration (superficial) velocity of the exhaust gas in the soot layer, and K is the rate coefficient of the soot oxidation surface reaction, which depends on the temperature T through a modified Arrhenius form

$$K = k_o T e^{-(E/RT)} \tag{2}$$

The initial condition for Eq.1. is that at $x = w$, $Y = Y_{\text{in}}(t)$.

Let $m(x)$ be the cumulative soot mass per unit of filter wall area from the wall surface ($z = 0$) up to a deposit height z = x. The total soot mass per unit area is M (that is, $M = m(w)$). The deposit density is related to the function $m(x)$ through the relations

$$m(x) = \int_0^x \rho(z)dz \Rightarrow \rho(x) = \frac{dm}{dx} \tag{3}$$

Using the stoichiometry of the soot oxidation reaction, a global mass balance leads to the following equation for the soot mass evolution

$$\frac{dM}{dt} = -\frac{M_c}{M_{ox}}\rho_g v(Y(w) - Y(0)) \tag{4}$$

where M_c and M_{ox} are the molecular weights of carbon and oxygen, respectively.

At this point appropriate balance laws for the state variables ρ(x), S(x) must be derived. Let us assume that $F_\rho(\rho,S,Y,x,t)$ and $S(\rho,S,Y,x,t)$ are the intrinsic rates of density and specific surface variation, respectively. The generalized explicit dependence of local variables on the above rates will be omitted in the following for the sake of presentation clarity. The main complication for the derivation of the balance equations is that, as the deposit thickness is reduced during the regeneration each (material) point of the deposit moves with its own velocity, lets say $\dot{x}(x, t)$. The material derivative (the derivative measured by an observer moving with the local deposit velocity) for any state variable would be equal to the intrinsic rate of the variable variation. This means that the following conservation equations can be written for the deposit density and specific surface area

$$\frac{D\rho}{Dt} = \frac{\partial\rho}{\partial t} + \dot{x}\frac{\partial\rho}{\partial x} = F_\rho \tag{5}$$

$$\frac{DS}{Dt} = \frac{\partial S}{\partial t} + \dot{x}\frac{\partial S}{\partial x} = F_S \tag{6}$$

The next step is to find a relation for the rate of movement of the deposit $\dot{x}(x, t)$. The soot mass balance for a moving control volume (actual length in this case), which has two edges $x_1(t)$ and $x_2(t)$ is

$$\frac{d}{dt}\int_{x_1(t)}^{x_2(t)} \rho(z, t)dz = \int_{x_1(t)}^{x_2(t)} F_{ox}dz \tag{7}$$

where F_{ox} is the local rate of soot oxidation (here taken to be negative), which can be computed from the local oxygen depletion rate and the stoichiometry of the oxidation reaction

$$F_{ox} = -\frac{M_c}{M_{ox}}KS\rho_g\rho Y \tag{8}$$

Using Leibnitz's rule and taking the limit $x_1 \to x_2$ (or equivalently using the Reynolds transport theorem in one spatial dimension), Eq. 7 is transformed to

$$\frac{\partial\rho}{\partial t} + \frac{\partial\dot{x}\rho}{\partial x} = F_{ox} \tag{9}$$

Applying the rule of product differentiation to the spatial derivative in Eq. 9 and using Eq. 5 the following relation is obtained

$$\rho\frac{\partial\dot{x}}{\partial x} = F_{ox} - F_\rho \tag{10}$$

Integrating the earlier equation between 0 and x using as boundary condition, the fact that the wall-deposit interface is motionless (that is, $\dot{x}(x = 0) = 0$) leads to

$$\dot{x} = \int_0^x \frac{F_{ox} - F_\rho}{\rho}dz \tag{11}$$

According to this model the deposit shrinks in two parallel ways: internal layers collapse leading to global movement of the deposit and interface layer extinction without deposit movement. A key question is how the evolution of the deposit thickness should be computed. A first choice is by the equation

$$M = \int_0^w \rho dz \tag{12}$$

The problem is that this equation is fulfilled for every value of w larger than the real one since the density is zero for $x>w$ so the smallest w, which fulfills Eq. 12 must be chosen. Alternatively w can be defined as the largest x value for which $\rho>0$.

To complete the formulation of the regeneration process model, the intrinsic variation rates of density F_ρ, and specific surface area F_s, must be explicitly given. These are constitutive laws depending on the deposit layer microstructure. To get an

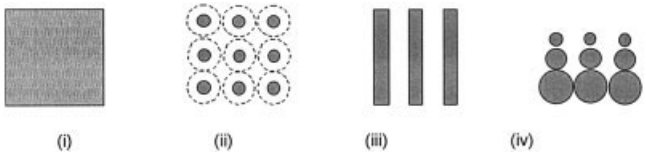

Figure 3. Simple microstructures for soot layer: (1) constant density model, (2) sphere in cell model, (3) cylindrical column model, and (4) columns of spherical particle column.

idea about their form we will derive them for some simple deposit structures at the particle level.

Particle level models

Constant density-constant specific surface area deposit

This is the deposit structure implied whenever no special consideration for the deposit microstructure is made (Figure 3). All the well-known models of regeneration have employed this structure. The constitutive laws for the variation rates are by definition equal to zero (that is, $F_\rho = F_s = 0$). It must be noted that this model is actually a lumped one and it has not a direct particle level analog. Although the density, in principle, can remain constant by changing the packing of the shrinking particles, it is not clear how the specific surface area of the shrinking soot primary particles could be maintained constant.

Sphere in cell model of deposit

This model is well known from the porous media and filtration literature.[15] According to this description the local structure of the deposit is represented by a spherical particle surrounded by a spherical cell of such radius that the ratio of the particle mass to this cell volume is equal to the local deposit density. As the particle size decreases due to oxidation, the local deposit density decreases too. Obviously, the local density is related to the local particle radius r through the relation

$$\frac{\rho}{\rho_o} = \left(\frac{r}{r_o}\right)^3 \tag{13}$$

where the index o implies initial conditions. The rate of particle radius decrease is related to the local reaction rate F_{ox} by

$$N\rho_s 4\pi r^2 \frac{dr}{dt} = F_{ox} \tag{14}$$

where N is the number of particles (cells) per unit volume, and ρ_s is the intrinsic density of soot. From geometrical considerations the following relation is obtained

$$\frac{\rho_o}{\rho_s} = N\frac{4}{3}\pi r_o^3 \tag{15}$$

Time differentiation of Eq. 13 leads to

$$F_\rho = \frac{d\rho}{dt} = \frac{\rho_o}{r_o^3} 3r^2 \frac{dr}{dt} \tag{16}$$

Elimination of the radius derivative from Eq. 14 and use of Eq. 15 leads to the final result

$$F_\rho = F_{ox} \tag{17}$$

It is well known that the specific area is inversely proportional to the particle size so

$$\frac{S}{S_o} = \frac{r_o}{r} \Rightarrow F_S = \frac{dS}{dt} = -S_o r_o r^{-2}\frac{dr}{dt} = -\frac{S_o}{3\rho_o}\left(\frac{\rho_o}{\rho}\right)^{4/3} F_{ox} \tag{18}$$

Alternatively, the specific area can be directly related to the deposit density as follows

$$\frac{S}{S_o} = \left(\frac{\rho_o}{\rho}\right)^{1/3} \tag{19}$$

As it will be shown this relation is much more descriptive for the deposit microstructure and very advantageous for computations than the use of the constitutive law in Eq.18.

According to this microstructural model there is no internal movement of the deposit ($\dot{x} = 0$), and the deposit thickness decreases only through extinction (its density goes to zero) of the surface layer. It is interesting to note that this model does not consider connectivity requirements of the deposit (that is, the deposit keeps its height even for small density). For this reason the model is more appropriate for the case of existence of a compact support for the combustible particles (for example, deep-bed filters, catalytic layer in the two-layer regeneration model in Konstandopoulos and Kostoglou[4]).

Cylindrical columns of soot

In this case the deposit is assumed to consist of soot columns (rods) having cylindrical cross section with radius r. The surface number density of columns is N_A. It is assumed that the radius of columns is close to the radius of primary soot particles so mass-transfer phenomena are not important and the deposit can be assumed to be homogeneous on the size scale of deposit thickness (a simple computation reveals that the distance between columns is much smaller than the thickness of the deposit). Eqs. 13, 14, and 15 of the previous case now take the following form

$$\frac{\rho}{\rho_o} = \left(\frac{r}{r_o}\right)^2 \tag{20}$$

$$N_A\rho_s 2\pi r \frac{dr}{dt} = F_{ox} \tag{21}$$

$$\frac{\rho_o}{\rho_s} = N_A\pi r_o^2 \tag{22}$$

Following a procedure similar to that of previous case the earlier equations can lead to the following result for the deposit density constitutive relation: $F_\rho = F_{ox}$. From Eqs. 20 to 22, it

can be found that the specific area-density relation now has the form

$$\frac{S}{S_o} = \left(\frac{\rho_o}{\rho}\right)^{1/2} \tag{23}$$

Although this model takes into account the connectivity of the deposit (through the columnar structure), its macroscopic features are the same with that of the previous one (that is, no internal motion of the deposit). The only difference between the two microstructural models is the exponent in the specific area-density relation (cf. Eqs. 19 and 23).

Columns of spherical particles

This is the most complicated model employed in the literature[11] to account for deposit microstructure evolution during regeneration. The deposit is assumed to consist of columns of spherical particles stacked one on top of the other. The main difference with the cylindrical columnar model is that now as each particle surface shrinks the column (and the deposit) looses its height. An additional assumption required for the continuum description of the deposit at this scale is that the deposit thickness be much larger that the soot primary particle radius r. The local deposit density can be found from the relation valid at the single particle scale

$$\rho = \frac{\Delta m}{\Delta x} \propto \frac{r^3}{r} = r^2 \tag{24}$$

which means that

$$\frac{\rho}{\rho_o} = \left(\frac{r}{r_o}\right)^2 \tag{25}$$

Considering that N (particle number/volume) and N_A (column number/surface) is related as $N = N_A/2r$, Eqs. 14 and 15 can be written as

$$N_A \rho_s 2\pi r \frac{dr}{dt} = F_{ox} \tag{26}$$

$$\frac{\rho_o}{\rho_s} = N_A \frac{2}{3} \pi r_o^2 \tag{27}$$

Using Eqs. 25, 26 and 27, after some algebra, one can find the following constitutive relation for this deposit microstructure

$$F_\rho = \frac{2}{3} F_{ox} \tag{28}$$

The following specific area-density relation is also obtained

$$\frac{S}{S_o} = \left(\frac{\rho_o}{\rho}\right)^{1/2} \tag{29}$$

In this case the deposit height is reduced both by surface layer extinction and by internal motion due to change of the connectivity between soot particles. Actually 2/3 of the soot oxidation rate contributes to deposit density reduction, and the rest 1/3 contributes to direct loss of height due to restructuring.

Generalization of constitutive rates

An important observation is that although four very different to each other discrete particle level models are considered, the information transmitted from this scale to the homogeneous deposit model employed for simulation can be assigned to just two parameters. To be more specific the constitutive laws for all the above microstructural models are of the type

$$F_\rho = \alpha F_{ox} \tag{30}$$

$$\frac{S}{S_o} = \left(\frac{\rho_o}{\rho}\right)^\beta \tag{31}$$

So it is logical to assume that the above relations with parameters α and β taking values between 0 and 1 represent a general continuum description of the deposit microstructure. The conservation equations for density and specific area can be written as

$$\frac{\partial \rho}{\partial t} = \alpha F_{ox} - \dot{x} \frac{\partial \rho}{\partial x} \tag{32}$$

$$\frac{\partial S}{\partial t} = -S_o \beta \rho_o^\beta \rho^{-1-\beta} \frac{d\rho}{dt} - \dot{x} \frac{\partial S}{\partial x} \tag{33}$$

$$\dot{x} = \int_0^x (1 - \alpha) \frac{F_{ox}}{\rho} dz \tag{34}$$

The above problem is a hyperbolic one, and its numerical solution in an Eulerian framework is difficult. On the other hand, it is ideally suited for solution using a Lagrangian approach. According to this, the following relations are valid on the characteristics defined by Eq. 34

$$\frac{d\rho}{dt} = \alpha F_{ox} \tag{35}$$

$$\frac{S}{S_o} = \left(\frac{\rho_o}{\rho}\right)^\beta \tag{36}$$

In this work it will be assumed that the temperature is uniform across the soot layer (small thermal Peclet number limit as it has been proven by Bissett[13]). This uniform temperature obeys the following conservation equation

$$(c_{pw} m_w + c_{ps} M) \frac{dT}{dt} = \Delta H \frac{dM}{dt} + G c_{pg} (T_{in} - T) \tag{37}$$

where c_{pw}, c_{ps}, c_{pg} are the specific thermal capacities of the wall, the soot and the exhaust gas, respectively, m_w is the wall mass per filtration area and ΔH is the heat of oxidation reaction.

Dimensionless Formulation

The following dimensionless variables are introduced

$$\bar{T} = T/T_o,\ \bar{Y} = Y/Y_o,\ \bar{G} = G/G_o,\ \bar{M} = M/M_o,\ \bar{\rho} = \rho/\rho_o,\ \bar{S} = S/S_o,\ \bar{x} = x/w_o,\ \bar{w} = w/w_o,$$

$$\bar{K}(T) = \frac{K(T)}{K(T_o)},$$

$$A = \frac{K(T_o) w_o \rho_o S_o}{v},$$

$$\tau = \frac{M_c}{M_{ox}} K(T_o) S_o \rho_{go} Y_o,$$

$$C_1 = \frac{G_o \Delta H}{c_{pw} m_w T_o K(T_o) S_o \rho_{go}},$$

$$C_2 = \frac{M_{ox} G_o c_{pg}}{M_c c_{pw} m_w K(T_o) S_o \rho_{go} Y_o},$$

$$C_3 = \frac{c_{ps} M_o}{c_{pw} m_w}$$

where T_o is the initial filter temperature, Y_o is the inlet oxygen mass fraction at $t = 0$, G_o is the exhaust mass flux (with respect to filtration area) at $t = 0$, M_o is the initial soot mass per unit filtration area, ρ_{go} is the exhaust density at $t = 0$ (from ideal gas law), and ρ_o, S_o are reference values for the density and surface area of the deposit, respectively. Using the new variables, the Lagrangian form of the problem that must be solved is

$$\frac{d\bar{Y}}{d\bar{x}} = \frac{1}{\bar{G}(\tau)\bar{T}} \bar{K}(\bar{T}) A \bar{\rho}^{1-\beta} \bar{Y} \tag{38}$$

$$\frac{d\bar{\rho}}{d\tau} = -\alpha \frac{1}{\bar{T}} \bar{K}(\bar{T}) \bar{\rho}^{1-\beta} \bar{Y} \tag{39}$$

$$\frac{d\bar{x}}{d\tau} = -\frac{(1-\alpha)}{\bar{T}} \int_0^{\bar{x}} \bar{K}(\bar{T}) \bar{\rho}^{-\beta} \bar{Y} dz \tag{40}$$

$$(1 + C_3 \bar{M}) \frac{d\bar{T}}{d\tau} = C_1 \bar{G}(\tau)(\bar{Y}_{in}(\tau) - \bar{Y}(0)) + C_2 \bar{G}(\tau)(\bar{T}_{in}(\tau) - \bar{T}) \tag{41}$$

with initial and boundary conditions

$$\bar{Y} = \bar{Y}_{in}(t) \text{ at } \bar{x} = \bar{w} \tag{42a}$$

$$\bar{\rho}(x, 0) = \bar{\rho}_o(\bar{x}) \tag{42b}$$

$$\bar{T}(0) = 1 \tag{42c}$$

Problem Solution

Simplified cases

Some simple solutions for the idealized case of constant exhaust flow rate, temperature and oxygen mass fraction and constant deposit temperature (slow regeneration) will be presented next for certain combinations of the parameters α, β.

Case 1 ($A \ll 1$)

In this case the oxygen depletion across the deposit is small in comparison to the oxygen concentration so the oxidation reaction has everywhere the same rate ($\bar{Y} = 1$). The following exact solutions can be found for a deposit with uniform initial density and $\beta \neq 0$

$$\bar{\rho} = (1 - \alpha\beta\tau)^{1/\beta} \tag{43}$$

$$\bar{M} = (1 - \alpha\beta\tau)^{1/\alpha\beta} \tag{44}$$

The point $\bar{x}(0)$ of the initial deposit evolves as

$$\bar{x} = \bar{x}(0)(1 - \alpha\beta\tau)^{(1-\alpha)/\alpha\beta} \tag{45}$$

In the limit $\beta \to 0$ the above equations take the form

$$\bar{\rho} = e^{-\alpha\tau} \tag{46a}$$

$$\bar{M} = e^{-\tau} \tag{46b}$$

$$\bar{x} = \bar{x}(0) e^{-(1-\alpha)\tau} \tag{46c}$$

This simple result is very revealing with respect to the meaning of the parameter α. The total soot mass evolution is independent of α. The role of α is to split the soot mass reduction rate between a density reduction and a deposit thickness reduction. So the deposit structure for the same deposit mass is a function of α. Directly measurable quantities, such as the pressure drop, depend (in addition to total soot mass) on deposit structure and, thus, on α as well. In the Appendix it is shown that the pressure-drop evolution during the regeneration is related primarily to the thickness evolution of the soot layer and not to its total mass.

Case 2 (α=0)

This is the constant density case corresponding to the widely used microstructural model (1).

The oxygen concentration across the deposit is $\bar{Y} = e^{A(\bar{x} - \bar{w})}$. The evolution of deposit thickness w, and the trajectory of a material point of the deposit can be found from the solution of the following differential equations, where it is noted that in this case $\bar{M} = \bar{w}$

$$\frac{d\bar{w}}{d\tau} = -\frac{1}{A}(1 - e^{-A\bar{w}}) \tag{47a}$$

$$\frac{d\bar{x}}{d\tau} = \frac{1}{A}(e^{-A\bar{w}} - e^{A(\bar{x}-\bar{w})}) \tag{47b}$$

Case 3 (α=1, β=1)

Although there is no analytical solution for this case, it is useful to reveal some aspects of the structure of the solution with respect to the subsequently developed numerical methods.

The value α=1 means that there is no internal motion of the deposit (similar to microstructure model 2), and so the Eulerian and Lagrangian approaches coincide. The partial-differential equation that must be solved is

$$\frac{\partial\bar{\rho}}{\partial\tau} = -e^{A(\bar{x}-\bar{w})} \tag{48}$$

The difficulty here arises from the fact that w is given implicitly by Eq. 12. A continuous tracking of the interface similar to that used for the internal movement is not possible so a discrete (step-wise) technique will be used. A uniform discretization in n points x_i ($x_o = 0$, $x_n = 1$) with spacing $h = 1/n$ is assumed in x direction. Initially, the deposit height is $w = x_n$. The surface position is assumed constant until the density of the surface layer ρ_n goes to zero. During this time interval the equations can be solved in closed form. The surface position is assigned to the next point $w = x_{n-1}$, and the procedure is repeated until the deposit is completely burnt out. The deposit evolution is computed by the following set of equations

$$\tau^{(j)} = \tau^{(j-1)} + \rho_{n+1-j}^{(j-1)} \tag{49a}$$

$$w^{(j)} = x_{n-j} \tag{49b}$$

$$\bar{\rho}_k^{(j)} = \rho_k^{(j-1)} - e^{A(x_k - w^{(j)})} \tag{49c}$$

where the superscript refers to the time-step, and the subscript to the spatial location. The value $j = 0$ corresponds to the initial conditions, and the indices take values: $1 \le j \le n$, $1 \le k \le n$.

General numerical approach

In the general case the deposit shrinks by combination of internal layer collapse and surface layer extinction so the numerical integration along the characteristics must be combined with the above Eulerian method for tracking of the interface. The set of equations that must be solved for the moving grid points and the deposit properties on them are (i = 0,1,2,..n)

$$\bar{Y}_i = \bar{Y}_{in}\exp\left[-A\frac{1}{\bar{G}\bar{T}}\frac{1}{2}\cdot\sum_{j=i+1}^{L}(\bar{K}_j\bar{\rho}_j^{1-\beta} + \bar{K}_{j-1}\bar{\rho}_{j-1}^{1-\beta})(x_j - x_{j-1})\right] \tag{50}$$

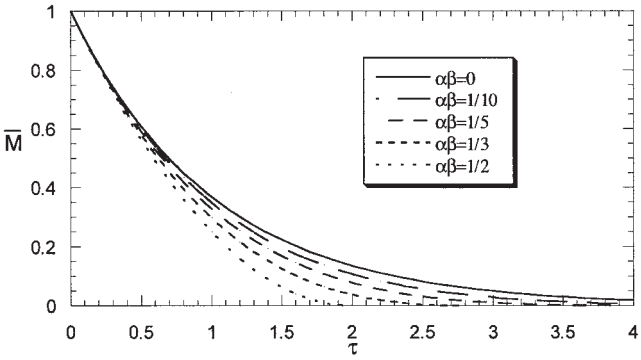

Figure 4. Evolution of the dimensionless soot mass $\bar{M}$ for slow regeneration with A = 0 and several values of the product $\alpha\beta$.

$$\frac{d\bar{\rho}_i}{d\tau} = -\alpha\frac{1}{\bar{T}}\bar{K}_i\bar{\rho}_i^{1-\beta}\bar{Y}_i \tag{51}$$

$$\frac{d\bar{x}_i}{d\tau} = -(1-\alpha)\frac{1}{2\bar{T}}\cdot\sum_{j=i+1}^{L}(\bar{K}_j\bar{\rho}_j^{-\beta}\bar{Y}_j + \bar{K}_{j-1}\bar{\rho}_{j-1}^{-\beta}\bar{Y}_{j-1})(x_j - x_{j-1}) \tag{52}$$

where $x_i(0) = x_{io}$ are the initial grid points.

The trapezoidal rule has been used for all the spatial integrations. The earlier system of ODE's is integrated numerically using an explicit Runge-Kutta integrator with self-adjustable integration step.[16] The surface is located at the grid point with index L. Initially L = n. At the moment the density of the surface layer goes to zero, the integration is stopped and the integrator restarts with a smaller number of equations and smaller value of L (by one). The procedure is repeated until L = 0. As the spatial grids get finer, the approximate (step-wise) position of the surface converges to the exact one.

Results and Discussion

Parametric study

A sensitivity analysis regarding the influence of the structural parameters α and β on the evolution of the soot layer during regeneration will be performed next. There are two distinct regeneration scenarios. In the first case the regeneration is so slow that the heat released from the reaction is convected by the flow before any increase of the filter wall temperature. For constant exhaust temperature the filter would have the same temperature also, and the system of equations can be simplified (solution of the heat equation is not needed). Furthermore, a uniform initial deposit is assumed.

First, the case of the insignificant oxygen consumption ($A \to 0$), which has been solved in closed form, is examined. Under this condition the density of the deposit retains its initial uniformity. The dimensionless total soot mass evolution is shown in Figure 4 for several combinations of α and β values.

For $\alpha = 0$ (constant density), the well-known exponential curve for first-order reaction is recovered. It is interesting to note that the soot mass evolution depends only on the product $\alpha\beta$ and not on each parameter separately. As the value of this

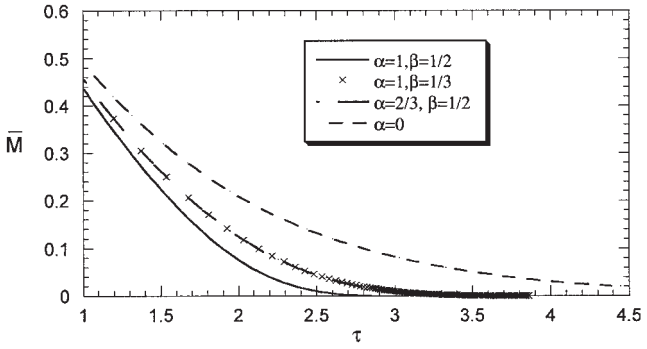

Figure 5. Evolution of the dimensionless soot mass $\bar{M}$ for slow regeneration with A = 1 and several combination of microstructure parameters α and β.

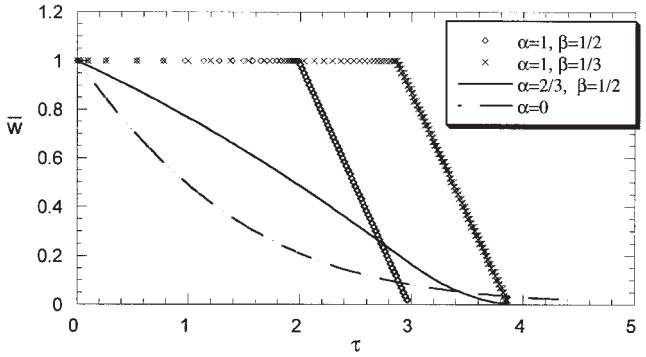

Figure 7. Evolution of the dimensionless soot layer thickness $\bar{w}$ for slow regeneration with A = 1 and several combination of microstructure parameters α and β.

product increases the deposit burns out faster. The increase of β accelerates the total reaction rate, because the specific surface area S increases with β for any given reduction of the density. On the other hand, as α increases density decreases, and S increases for a constant β value.

The total soot mass evolution for the case A = 1 (mild oxygen consumption) is shown in Figure 5. The influence of the structural parameters is restricted only to the final stages of deposit combustion. Again the combustion rate increases with the increase of the parameters α and β. It is interesting to remark that the curves ($\alpha = 2/3$, $\beta = 1/2$) and ($\alpha = 1$, $\beta = 1/3$) which have the same value of the product are indistinguishable.

The corresponding curves for the case A = 4 (strong oxygen consumption) are shown in Figure 6. Initially, all deposits have the same evolution (zero-order reaction with rate equal to the oxygen flow rate), and only when the deposit gets thin enough to leave unburned oxygen the structure plays a role. In other words, there is a combustion zone in the deposit with thickness proportional to 1/A. In case of a deposit thicker than this combustion zone the microstructure does not influence total combustion rate. When the boundaries of the combustion zone reach the filter wall the microstructure comes into play.

To summarize the effect of microstructure on the total deposit mass evolution is restricted to cases of small oxygen consumption, and it is mainly through the product $\alpha\beta$. The situation is quite different as regards the evolving structure of the soot layer, which depends strongly on the parameters α, β separately (not just on their product) and regardless of the oxygen consumption level. The evolution of the dimensionless deposit thickness for the case A = 1 and several combinations of parameters α, β are shown in Figure 7.

For $\alpha = 1$, the thickness remains constant as the density reduces until the time of zeroing of the surface layer density, and then decreases linearly until total extinction of the soot. The starting time of this linear reduction depends on β, but its rate does not. If α is different from 1 the deposit collapse starts from time zero. Initially, the collapse rate is larger for α smaller, but at the last stages the order is reversed. Increase of β leads to increased collapse rate, but its effect is smaller as α gets smaller. The maximum β dependence exists for $\alpha = 1$, and there is no β dependence at all for $\alpha = 0$.

Figure 8 is similar to Figure 7, but it refers to A = 4. Qualitatively, the curves are similar to those for A = 1. An important observation is that the slope of the thickness reduction rate for $\alpha = 1$ is equal to 1/A in dimensionless coordinates, which means that it is independent from the reaction rate. This 1/A dependence holds for any value of A and has to do with the reaction rate gradient close to the deposit surface, and it is not related with the similar dependence for the $\alpha = 0$, $A \gg 1$ case, which is due to oxygen depletion. The evolution of the soot

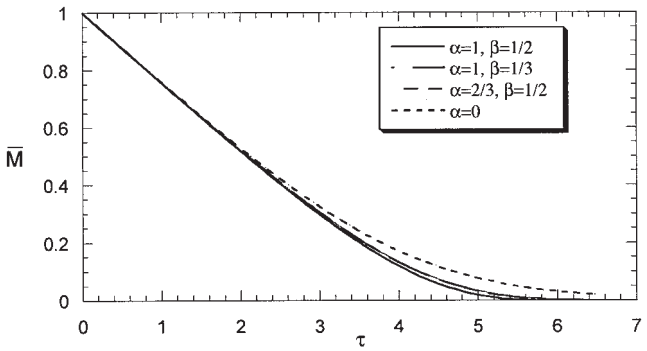

Figure 6. Evolution of the dimensionless soot mass $\bar{M}$ for slow regeneration with A = 4 and several combination of microstructure parameters α and β.

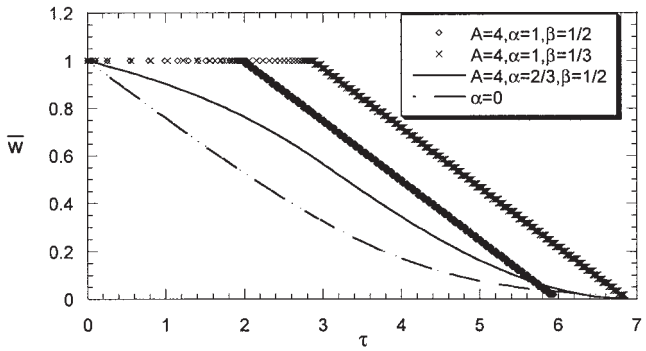

Figure 8. Evolution of the dimensionless soot layer thickness $\bar{w}$ for slow regeneration with A = 4 and several combination of microstructure parameters α and β

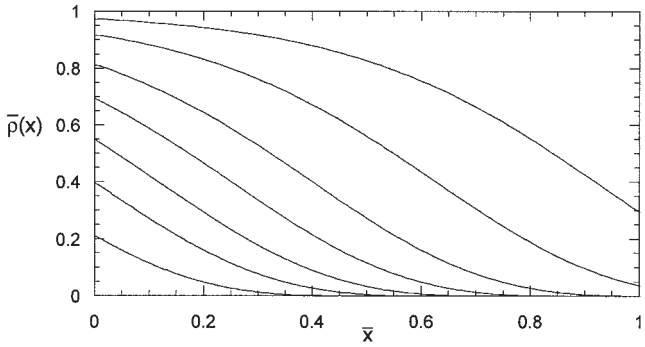

Figure 9. Dimensionless density profile in the soot layer at several times for $\alpha = 1$, $\beta = 1/3$, A = 3 (slow regeneration).

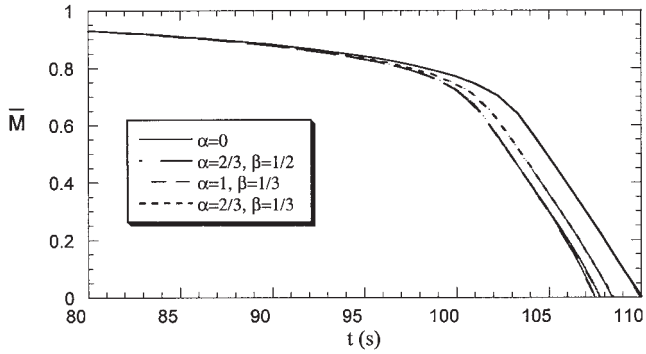

Figure 11. Evolution of the dimensionless soot mass $\bar{M}$ for the fast regeneration scenario with several combination of microstructure parameters α and β.

density profiles across the deposit is shown for two typical cases in Figure 9 and Figure 10, respectively.

In the first case ($\alpha = 1$, A = 3, $\beta = 1/3$) there is no internal deposit movement, and it is shown clearly how density decreases until it reaches the zero value at the surface. After this moment the deposit starts shrinking having always a not clearly defined surface with density approaching zero. In the case of internal deposit movement ($\alpha = 2/3$, A = 4, $\beta = 1/2$) the deposit starts shrinking before the zeroing of surface density occurs, so for some time it has a finite surface density. Then the surface density goes to zero but the surface is clearly better defined (larger density gradient) than in the previous case.

The second regeneration scenario studied here is the fast regeneration, where an increasing temperature of the exhaust gas leads to an initially slow reaction, which is accelerated gradually. At some point the heat produced by the reaction cannot be convected by the flow so ignition occurs leading to fast burning of the soot layer. This mode of the regeneration is more complicated than the previous one since it combines periods of insignificant and complete oxygen depletion.

A regeneration case similar to that of Bissett and Shadman[12] is employed here to examine the sensitivity with respect to the deposit microstructure. The following are the values of parameters and the inlet conditions used: $T_o = 600$ K, E/R = 18,000 K, $M_o = 20$ g/m^2, $m_w = 238$ g/m^2, $Y_{in}(t) = Y_o = 0.1$, $G(t) = G_o = 0.05$ kg/(m^{2}s), $T_{in}(t) = 600+200*(1-\exp(t/100))$ K (t in seconds). For demonstration purposes the product $S\rho_o k_o = 3\rho_o k_o/r_o\rho_s$, was set at the value $12.12 \cdot 10^9$ 1/(sK), based on the individual parameter values in Bissett and Shadman.[12] The individual parameters of the product could vary according to the type of soot, soot layer structure and reactivity, while only their product value is determining the soot oxidation behavior. For a soot layer density[8] of $\rho_o = 140$ kg/m^3, with $\rho_s = 2{,}000$ kg/m^3 and $r_o = 20$ nm, this leads to a value of $k_o = 1155$ m/(sK).

The evolution of the deposit mass during fast regeneration for several values of parameters α and β is shown in Figure 11. The main difference between the several cases is a time lag of at most 2.5 s. Initially, the reaction is slow and the oxygen depletion is small. This means (according to the slow regeneration case analysis) that the reaction rate is different for each microstructural model leading to different ignition moment. After the ignition, oxygen depletion is complete so the total combustion rate does not depend on the microstructure and the curves in Figure 11 are parallel to each other. The mass evolution depends mainly on the product $\alpha\beta$ as is shown by comparing cases ($\alpha = 2/3$, $\beta = 1/2$) and ($\alpha = 1$, $\beta = 1/3$), and in general ignition is occurring faster as the product $\alpha\beta$ increases. The corresponding evolution of the deposit thickness is depicted in Figure 12.

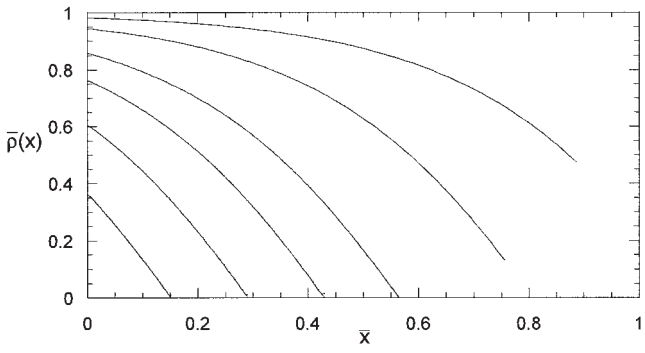

Figure 10. Dimensionless density profile in the soot layer at several times for $\alpha = 2/3$, β=1/2, A = 4 (slow regeneration).

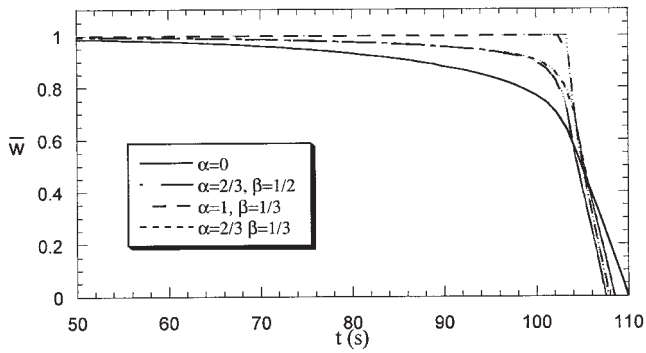

Figure 12. Evolution of the dimensionless layer thickness $\bar{w}$ for the fast regeneration scenario with several combination of microstructure parameters α and β.

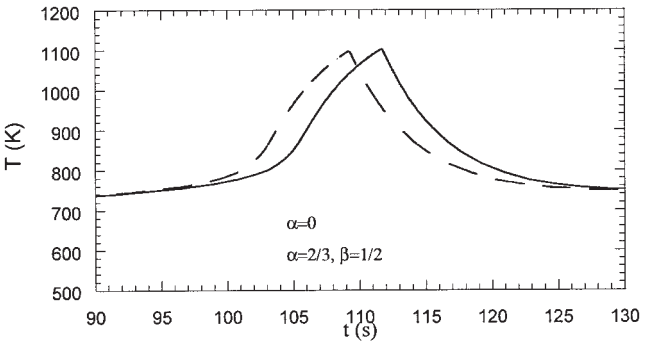

Figure 13. Evolution of filter temperature for the fast regeneration scenario with $\alpha = 0$, and $\alpha = 2/3$, $\beta = 1/2$.

Here, the differences between the microstructural models are beyond the simple time shift observed for the total mass. In general, the thickness is initially larger than that of the conventional model with $\alpha = 0$, but after some time it decreases with a larger rate leading to a faster total soot deposit extinction. The evolution of the filter temperature is shown in Figure 13 for the two most important cases that of constant density ($\alpha = 0$) and a columnar deposit of spherical particles ($\alpha = 2/3$, $\beta = 1/2$).

It is obvious that the temperature curves are exactly the same except for a time shift. The earlier results can be generalized by making the statement that any change to the effective reaction rate pre-exponential factor leads to a time shift of the temperature evolution curve without altering its shape. The density profiles across the soot layer during regeneration for the case ($\alpha = 2/3$, $\beta = 1/2$) are shown in Figure 14.

Initially, the density decreases uniformly, and the thickness decreases due to the internal motion of the deposit (t = 101.41 s). Then the reaction is restricted to the region close to the surface of the deposit leading to a sharp variation of density close to the surface (t =105.18 s). Finally, the reaction occurs on the surface leaving constant the density (almost uniform) and decreasing the thickness (t ≥106.21 s).

Comparison to Experiments

In order to check the consistency of the developed microstructural oxidation model, well-controlled experiments have been conducted with soot deposits grown on sintered metal filter disks exhibiting cake filtration characteristics. Such filter media are currently under consideration for application in heavy duty diesel vehicles.[17] The experimental reactor set-up has been described in detail in Konstandopoulos et al.[2]

A modern Euro III common rail 1.9 L diesel engine operated on low sulfur (< 50 ppm) fuel at steady state has been employed as the source of soot. A regulated constant flow sidestream from the exhaust was driven at two filtration velocities (8 and 16 cm/s) through the 40 mm filter disk samples until an amount of soot on the order of 12 g/m^2 of filter area was obtained. The filtration velocities employed are high with respect to those of typical honeycomb, wall flow filters (usually 2 – 4 cm/s), but quite appropriate for sintered metal media. On the basis of the mass transfer Pe number (which in both cases was in the convection dominated regime), it could be expected that the porosity of both deposits (that grown at 8 cm/s, and that at 16 cm/s) would be the same as shown in Konstandopoulos et al.[8] for deposits grown in cordierite filters (but with smaller filtration velocities than those here). However, as deposit compaction could also occur at the high filtration velocities, these experiments provided some typical soot deposits expected to grow on sintered metal filters. After soot loading of the filters a temperature programmed oxidation (at the rate of 3 C/min) of the soot deposit with a 10% oxygen in nitrogen flow of 2.5 std l/min was carried out.

Soot conversion was obtained by integrating the evolved CO_2 and CO signals during the soot oxidation. The CO selectivity was about 0.3, but it does not influence the soot conversion as the reactor operates in the slow regeneration regime where there are no exotherms, and the soot deposit temperature follows the evolution of the reactor temperature.

A model of a soot deposit made of spherical primary particles of 32 nm in dia.[8] in columnar arrangement has been employed ($\alpha = 2/3$, $\beta = 1/2$). Soot deposit packing density was kept constant at the value corresponding to the prevailing Peclet number.[8] It is commonly recognized[18,19] that a "true" activation energy for diesel soot does not exist. In this work we followed past experience, based on fitting mathematical models of the regeneration process to experimental data[5] for assigning an activation energy to the oxidation of diesel soot on sintered metal disks. Accordingly, for the particular engine-fuel combination employed in our laboratory, a reduced activation energy E/R = 21,700 K had been found for noncatalytic soot oxidation on filters made of a proprietary ceramic material, and this value was employed here. The only fitted parameter was the pre-exponential factor for the 8 cm/s grown deposit, which was found to be 70 m/(sK) by least-squares minimization. The model was then run with these parameters for the 16 cm/s grown deposit. Figure 15 depicts the soot conversion vs. temperature of the 8 cm/s grown deposit, while Figure 16 that of the 16 cm/s along with the model calculations, establishing the consistency of the model. Further similar experiments are underway.

Discussion

Although the framework for continuous representation of soot deposit microstructure developed here is employed for relatively simple processes, it can accommodate much more

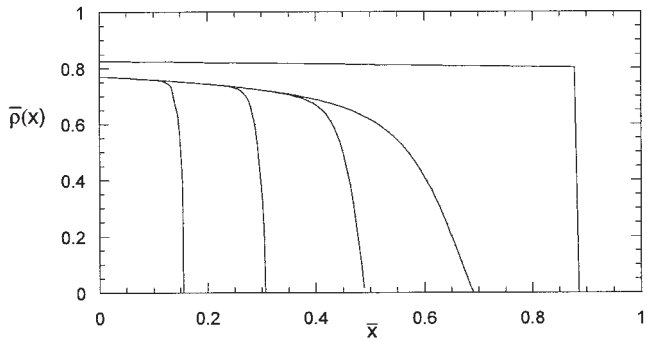

Figure 14. Dimensionless density profile in the soot layer at several times for $\alpha = 2/3$ and $\beta = 1/2$, (fast regeneration).

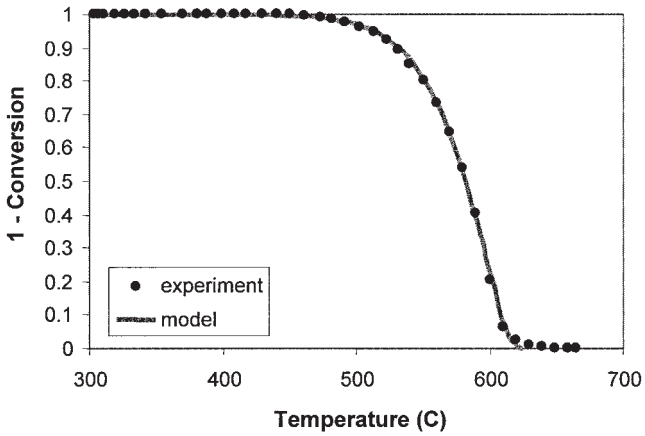

Figure 15. Soot conversion of deposit grown at 8 cm/s filtration velocity.

Experiment vs. model.

complicated phenomena. The parameters α, β can be varied locally in several regions of the deposit (deep bed and cake regions can be defined in this way). Also, these parameters can depend on the local density allowing acceleration of the deposit collapse for small density.

The initial soot distribution profile in the filter structure could be specified from filtration theory[2] or more advantageously, the filtration step can be incorporated into this framework. The reaction rate can be different in different regions of the deposit to account for a possible spatial distribution of the catalyst and reproduce, for example, the so-called two-layer model[4] of a catalytic filter or more general microstructural soot-catalyst contact models. These will be presented in a future publication.

A few comments are in order regarding the influence of the type of soot produced from an engine on the microstructure evolution of the soot cake. Depending on exhaust temperature, organic components from the lubrication oil and/or the fuel could condense on the soot particles and form the so-called soluble organic fraction (SOF) of diesel particulate. This is typically a phenomenon occurring upon dilution of the exhaust, sometimes leading to the formation of additional particles, the so-called nucleation mode.[20] A high SOF content soot is sometimes referred to as "wet soot" while a low content SOF as "dry soot". It should be noted although that reference to SOF content of diesel particulate matter almost always implies particulate matter sampled on a Teflon-coated filter after a relatively long residence time, dilution process in a dilution tunnel at a temperature of 52°C, as the legislated sampling protocols stipulate. Under engine operation at low exhaust temperatures, capillary condensation (due to the Gibbs-Kelvin effect) could occur on predeposited particles inside a diesel particulate filter, or even some direct oil-droplet deposition.[21] A very long timescale would be required for the latter phenomenon to lead to appreciable SOF amount in the filter. As exhaust temperature rises, evaporation and re-emission of that SOF would occur, leading to an increase in the accessible carbon surface area. It should be recalled that sampling lines and Flame Ionization analyzers for hydrocarbon emissions measurements from the exhaust are typically operating at 190°C to avoid condensation-induced sampling artifacts. In studies of diesel particulates under raw exhaust conditions using gravimetric raw exhaust sampling techniques[22] it was observed that at an exhaust temperature of 350 °C no particle-bound SOF was present. Any amount of SOF would, therefore, evaporate before any thermal soot oxidation would take place, and this continuum model would still be applicable. Within this formalism any influence of SOF condensation in the DPF is accommodated in the initial density profile distribution $\rho(x)$, and the microstructural parameters α and β. Most modern DPF systems are preceded by a diesel oxidation catalyst (DOC) which is employed to oxidize exhaust hydrocarbons (injected in the engine cylinder or in the exhaust), and, thus, raise the exhaust temperature to the levels needed for DPF regeneration. The DOC almost eliminates any SOF that might be present on the soot particles and it is, therefore, expected that the aforementioned SOF effects (if any) on the soot cake microstructure will become of less significance.

The incorporation of the microstructural continuum model locally into a single channel simulation is feasible, but it will be quite demanding in terms of the computational time required. A more immediate use of the microstructural model developed here with respect the overall filter simulation is as a prototype for the development of appropriate reduced models with fewer state variables to describe the deposit evolution. The simplest model of this type is the constant density- evolving thickness currently employed in most studies. The next step should be an evolving mean density-evolving thickness model (that is, a model based on two state variables). The evolution equations for this reduced model can be developed on the basis of this continuum microstructural model.

Conclusions

A continuum 1-D (across the deposit) model for the soot deposit evolution during the DPF regeneration process is developed here. The continuum model contains some constitutive laws (rates), which can be found by particle level models. It was found that these laws have a relatively simple form with just two adjusted parameters for a fairly large range of particle level dynamics. Special numerical algorithms have been developed for the solution of the deposit evolution problem, which

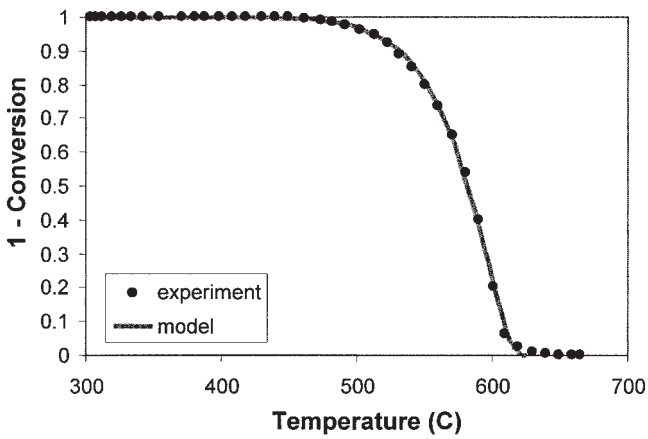

Figure 16. Soot conversion of deposit grown at 16 cm/s filtration velocity.

Experiment vs. model.

is complicated due to the combined shrinking by the intra-deposit combustion and surface layer extinction.

The results show that for the case of the slow regeneration the deposit microstructure (represented by the two parameters of the constitutive law) influences the total soot combustion rate only for the case of small oxygen depletion across the deposit. In the case of fast regeneration, the deposit microstructure influences only the moment of ignition by a few seconds leaving the shape of the mass and temperature evolution without changes. In both cases the height of the deposit thickness (which can be strongly related with the pressure drop in the filter) is much more sensitive to the microstructural parameters than its total mass. This work can be extended/exploited in two ways: To serve as the basic formulation for the development of complicated deposit level models (loading phase, deep bed regions, catalytic layer regions, interaction between the layer, and so on.), and as benchmarking for the development of lumped local deposit models to be incorporated in single channel module.

Acknowledgments

Partial support for this research has been provided by the European Commission GROWTH program, through the COMET project (Contract number: G3RD-CT-2002-00811).

Notation

A, C_1, C_2, C_3 = dimensionless parameters
c_{pw} = specific heat capacity of filter wall material
c_{ps} = specific heat capacity of soot
c_{pg} = specific heat capacity of exhaust gas
E = activation energy for soot oxidation
F_{ox} = soot oxidation rate
F_ρ = soot layer density variation rate
F_S = specific surface area variation rate
K = soot oxidation rate constant
k_o = pre-exponential factor for soot oxidation
m_w = filter wall mass per unit filtration area
M_c, M_{ox} = molecular weights of soot and oxygen, respectively
M = soot mass per unit filtration area
N = volume number of structural units per unit
N_A = number of structural units per unit surface
r = characteristic size of the structural unit of the soot layer
S = specific surface area (per unit mass) of soot layer
T = temperature
T_o = filter and gas temperature at t = 0
v = superficial filtration velocity
w = soot layer thickness
Y = oxygen mass fraction in exhaust gases

Greek letters

α, β: = generalized soot layer structural descriptors (see Eqs. 30 and 31)
ΔH = heat of soot oxidation reaction (per unit mass of soot)
ρ = soot layer density
ρ_g = exhaust gas density
ρ_s = intrinsic soot density
τ = dimensionless time
-Subscript o denotes the initial value
-Overbar denotes dimensionless quantity

Literature Cited

1. http://www.dieselnet.com, accessed on Oct. 3, 2003.
2. Konstandopoulos AG, Kostoglou M, Skaperdas E, Papaioannou E, Zarvalis D, Kladopoulou E. Fundamental studies of diesel particulate filters: transient loading, regeneration and aging. Society of Automotive Engineers (SAE) Tech. Paper No. 2000;01:1016.
3. Bissett EJ. Mathematical model of the thermal regeneration of a wall-flow monolith diesel particulate filters. *Chem Eng Sci*. 1984;39:1233-1244.
4. Konstandopoulos AG, Kostoglou M. Periodically reversed flow regeneration of diesel particulate traps. Society of Automotive Engineers (SAE) Tech. Paper No. 1999;01:0469.
5. Konstandopoulos AG, Kostoglou M. Reciprocating flow regeneration of soot filters. Combustion and Flame. 2000;121:488-500.
6. Kostoglou M, Housiada P, Konstandopoulos AG. Multi-channel simulation of regeneration in honeycomb monolithic diesel particulate filters. *Chem Eng Sci*. 2003;58:3273-3283.
7. Konstandopoulos AG, Kostoglou M, Housiada P, Vlachos N, Zarvalis D. Multichannel simulation of soot oxidation in diesel particulate filters. Society of Automotive Engineers (SAE) Tech. Paper No. 2003;01:0839.
8. Konstandopoulos AG, Skaperdas E, Masoudi M. Microstructural properties of soot deposits in diesel particulate filters. Society of Automotive Engineers (SAE) Tech. Paper No. 2002;01:1015.
9. Tassopoulos M, O'Brien JA, Rosner DE. Simulation of microstructure/mechanism relationships in particle deposition. *AIChE J*. 1989;35,967-980.
10. Houi D, Lenormand R. Particle deposition on a filter medium. In: Family F, Landau DP. Kinetics of Aggregation and Gelation. Amsterdam: North-Holland, 1984:173-176.
11. Shadman F. Kinetics of soot combustion during regeneration of surface filters. *Comb Sci and Technol*. 1989;63:183-191.
12. Bisset EJ, Shadman F. Thermal regeneration of diesel-particulate monolithic filters. *AIChE J*. 1985;31:753-758.
13. Bissett EJ. Thermal regeneration of particle filters with large conduction. *Math Modeling*. 1985;8:1-18.
14. Haralampous O, Koltsakis GC. Intra-layer temperature gradients during regeneration of diesel particulate filters. *Chem Eng Sci*. 2002;57:2345-2355.
15. Tien C. Granural filtration of aerosols and hydrosols. New York: Butterworths; 1989.
16. Press WH, Flannery BP, Teukolsky SA, Vetterling, W.T. Numerical recipes: *The Art of Scientific Computing*. New York: Cambridge University Press; 1989.
17. Frank W, Himmel M, Hüthwohl G, Neumann P. *Sintered Metal Particulate Filter to Meet Life Cycle Requirements of Commercial Vehicles*. In: Steinmetz E. Minimierung der Partikelemissionen von Verbrennungsmotoren. Essen: Expert-Verlag; 2004.
18. Neeft JPA, Nijhuis X, Smakman E, Makkee M, Moulijn JA. Kinetics of the oxidation of diesel soot. *Fuel*.1997;76:1129-1136.
19. Stanmore BR, Brilhac JF, Gilot P. The oxidation of soot: a review of experiments, mechanisms and models. *Carbon*. 2001;39:2247-2268.
20. Kittelson DB. Engines and nanoparticles: a review. *J of Aerosol Sci*. 1998;29:575-588.
21. Bardasz E, Mackney D, Britton N, Kleinschek G, Olofsson K, Murray I, Walker AP. Investigations of the interactions between lubricant-derived species and aftertreatment systems on a state-of-the-art heavy duty diesel engine. Society of Automotive Engineers (SAE) Tech. Paper No. 2003;01:1963.
22. Konstandopoulos AG, Gratz LD, Johnson JH, Bagley ST, Leddy DG. Ceramic particulate traps for diesel emissions control-effects of a manganese-copper fuel additive. Society of Automotive Engineers (SAE) Transactions. 1988;97:37-53.

Appendix

Relation between pressure drop and deposit microstructure during regeneration

The pressure drop can be computed directly if the flow resistance:

$$K_p = \frac{\Delta P}{v\mu}$$

of the deposit is known. The dimensionless flow resistance is given from the relation

$$\bar{K}_P = \frac{K_P}{K_{Po}} = \left[\int_0^{\bar{w}} \frac{f(\varepsilon_o)}{f(\varepsilon)} \left(\frac{r_o}{r} \right)^2 d\bar{x} \right]^{-1} \tag{A1}$$

where the subscript o denotes properties of the initial (uniform) deposit, f is the Kuwabara function, and r is the characteristic size of the particles in the deposit. The parameters α, β are not sufficient to infer the evolution of the characteristic size r, and a particular structure must be assumed. In the limit of an open deposit (that is, $\varepsilon \rightarrow 1$) the following approximation is valid

$$\frac{f(\varepsilon_o)}{f(\varepsilon)} = \frac{\rho}{\rho_o} \tag{A2}$$

Using this approximation and employing the structural models (1), (3), (4) for the characteristic size evolution leads to the interesting result

$$\bar{K}_p = \bar{w}^{-1} \tag{A3}$$

This relation shows why as regards pressure drop, the thickness of the soot layer is more important than its mass. The respective relation for model (2), which corresponds to deep bed filtration is

$$\bar{K}_P = \left[\int_0^{\bar{w}} \left(\frac{\rho}{\rho_o} \right)^{1/3} d\bar{x} \right]^{-1} \tag{A4}$$

Received Manuscript received Dec. 20, 2003, and revision received Dec. 19, 2004.